Strain Rate Dependent Analysis of a Polymer Matrix Composite Utilizing a Micromechanics Approach

ROBERT K. GOLDBERG*
NASA Glenn Research Center
Mail Stop 49-7
21000 Brookpark Rd.
Cleveland, OH 44135, USA

DONALD C. STOUFFER
University of Cincinnati
Department of Aerospace Engineering and Engineering Mechanics
Cincinnati, OH 45221-0070, USA

ABSTRACT: A research program is in progress to develop strain rate dependent deformation and failure models for the analysis of polymer matrix composites subject to high strain rate impact loads. The Ramaswamy–Stouffer viscoplastic constitutive equations for metals have been modified to model the strain rate dependent inelastic deformation of ductile polymers, including hydrostatic stress effects. These equations have been incorporated into a mechanics of materials based micromechanics model that was developed to analyze uniaxial composites at various fiber orientation angles. The Hashin failure criteria have been implemented into the micromechanics to predict ply failure strengths. The deformation response and ply failure strengths for the representative composite AS4/PEEK have been successfully predicted for a variety of fiber orientations and strain rates.

KEY WORDS: polymer matrix composites, micromechanics, viscoplasticity, strength, constitutive equations, impact.

INTRODUCTION

NASA GLENN RESEARCH Center has an ongoing research program to investigate the feasibility of developing jet engine fan containment systems composed of polymer matrix composite materials. To design a composite containment system, the ability to correctly predict the strain rate dependent deformation and failure behavior of these

*Author to whom correspondence should be addressed. E-mail: Robert.K.Goldberg@grc.nasa.gov

0021-9983/02/07 0773–22 $10.00/0 DOI: 10.1106/002199802024613

composites under high rate loading conditions is required. Furthermore, composites composed of relatively ductile matrix materials are more likely to be used for containment applications due to their energy absorbing capabilities. As a result, an analytical model must have the capability to account for nonlinearities and rate dependence in the material response.

Experimental techniques to characterize the behavior of polymer matrix composites under low strain rate loading conditions have been well established for many years. Furthermore, numerous analytical methods have been developed to model the deformation and failure behavior of composites under quasi-static loads. However, experimental techniques and analytical procedures for characterizing and modeling these materials under high strain rate conditions are still under development.

Several experimental studies have been performed by prior researchers with the goal of determining the effects of strain rate on the material properties and response of polymer matrix composites. Harding and Welsh [1] conducted tensile tests using a split Hopkinson bar on unidirectional graphite–epoxy composites with a [0°] fiber orientation. The elastic modulus and fracture strength obtained from these tests displayed little variation with strain rate. Since the response of a [0°] composite is primarily fiber dominated, these results indicated that the graphite fibers in tension had little strain rate dependence.

Daniel et al. [2,3] utilized expanding ring tests to examine the effects of strain rate on the longitudinal, transverse and shear properties of a unidirectional graphite–epoxy composite. From these experiments, it was determined that the material properties along the fiber direction of the composite showed little variation with strain rate, but the transverse and shear properties showed significant variation with strain rate. Since the transverse and shear response of a unidirectional composite is matrix dominated, the results indicated that for a carbon fiber reinforced polymer matrix composite, the material properties of the polymer matrix are strain rate dependent and drive the rate dependence of the composite.

Efforts have been made by prior researchers to model the rate dependent deformation response of polymer matrix composites. For example, Weeks and Sun [4] developed a macromechanical, rate dependent constitutive model to analyze the inelastic response of a carbon reinforced thermoplastic. A plastic potential function was used to compute the inelastic strains, and a scaling function was defined to model the variation of the response due to the varying fiber orientation angle of a single ply. The rate dependence of the composite was captured by varying the material constants as a function of strain rate. Thiruppukuzhi and Sun [5] later modified this technique in order to directly incorporate the rate dependence of the material response into the constitutive model. Micromechanics methods have also been applied to the problem. For example, Aidun and Addesio [6] developed a nonlinear elastic constitutive model to simulate the inelastic response of the polymer matrix. The equations were then implemented within a micromechanics model to compute the nonlinear deformation response of the composite.

A variety of failure criteria have been developed to predict the ply level ultimate strength in polymer matrix composites. Several "classic" criteria have been used, as detailed in texts such as those by Agarwal and Broutman [7], Daniel and Ishai [8] and Staab [9]. Simple criteria, such as Maximum Stress or Maximum Strain, simply compared macroscopic (ply level) stresses (or strains) in each coordinate direction to maximum values. More sophisticated criteria, such as Tsai–Hill and Tsai–Wu, utilized quadratic (and tensor in the

case of Tsai–Wu) combinations of the stresses to account for stress interaction. However, none of these criteria accounted for specific local failure mechanisms.

Researchers such as Hashin [10], Chang [11] and Rotem [12] developed failure models that utilized quadratic combinations of the macroscopic stresses to approximate local failure mechanisms, such as fiber failure or matrix cracking. These models have been used to predict impact failure in composites by Yen [13], Banerjee [14] and Langlie and Cheng [15], among others. The advantage of using this type of failure criteria was that by identifying specific local failure mechanisms, property degradation models could be developed to allow for reductions in specific material properties as loading took place.

This paper describes the development of strain rate dependent, inelastic constitutive equations to model the deformation response of a ductile polymer and the implementation of these equations into a mechanics of materials based micromechanics method. The incorporation of the Hashin failure criteria into the micromechanics model is also discussed. Verification studies for the deformation and ply strength models are presented for a representative composite system composed of AS-4 fibers in a PEEK thermoplastic matrix.

POLYMER CONSTITUTIVE EQUATIONS

Overview and Assumptions

Polymers are known to have a strain rate dependent deformation response that is nonlinear above about one or two percent strain. Traditionally, viscoelastic models have been used to capture this behavior from a phenomenological point of view [16]. Polymer deformation has been found to be due to the motion of molecular chains, and the resistance to this flow [17]. For this study, constitutive equations for ductile polymers that capture the deformation mechanisms of the material have been developed.

Specifically, the Ramaswamy–Stouffer state variable equations [18] have been modified to simulate the polymer deformation response. This model was originally developed to simulate the rate dependent, viscoplastic deformation response of metals above about one-half of the melting temperature. However, there is some physical motivation in utilizing state variable models that were developed for metals to analyze the nonlinear deformation response of polymers. For example, Ward [17] defined the ''yield stress'' in polymers as the stress level where the stress–strain curve becomes flat, and specified that this point occurs when the inelastic strain rate equals the applied strain rate in constant strain rate tensile tests. The identical definition has been used to define the ''saturation stress'' in metals [18]. Furthermore, in metals a ''back stress'' has been defined which represents the orientation dependent resistance to slip resulting from the piling up of dislocations under a shear stress at a barrier, and the repelling action caused by the atomic forces acting between the dislocations [18]. Similarly, Ward [17] defined an ''internal stress'' which represents the resistance to molecular flow during inelastic straining. In both cases, the net stress producing inelastic deformation is related to the difference between the applied stress and ''internal stress'' or ''back stress,'' and both the ''internal stress'' and ''back stress'' are defined as evolving with increasing strain. Polymers have been modeled previously using viscoplastic equations by authors such as Valisetty and Teply [19], Zhang and Moore [20], who modified Bodner's viscoplastic model [21], and Bordonaro [22], who modified Krempl's Viscoplasticity Theory Based on Overstress.

In developing state variable constitutive equations, a single unified strain variable is defined to represent all inelastic strains [18], and the effects of plasticity, viscoelasticity and creep are not separated. Furthermore, in the state variable approach inelastic strains are assumed to be present at all values of stress, and there is no defined yield stress or onset of inelasticity. The inelastic strains are merely assumed to be very small compared to the elastic strains at low stress levels. State variables are defined to represent the macroscopic average effects of the deformation mechanisms. The state variables are assumed to evolve with stress and inelastic strain.

Several significant limitations in using state variable equations developed to analyze metals in the modeling of polymers have been defined. The nonlinear strain recovery observed in polymers during unloading is not simulated during the current study. Furthermore, phenomena such as creep, relaxation and high cycle fatigue are not considered in the development and usage of the constitutive equations. Additionally, small strain conditions are assumed, and temperature effects are neglected. None of these restrictions were considered to be significant for the analyses conducted in this study. Finally, the constitutive equations utilized in this study are most likely only valid for ductile polymers, due to the fact that a significant amount of nonlinearity in the stress–strain response is assumed.

Flow and Evolution Equations

In the modified Ramaswamy–Stouffer model, the inelastic strain rate, $\dot{\varepsilon}_{ij}^{I}$ is defined as a function of the deviatoric stress, s_{ij}, and tensorial internal stress state variable Ω_{ij} in the form:

$$\dot{\varepsilon}_{ij}^{I} = D_0 \exp\left[-\frac{1}{2}\left(\frac{Z_0^2}{3K_2}\right)^n\right]\frac{s_{ij}-\Omega_{ij}}{\sqrt{K_2}} \tag{1}$$

where D_0 is a material constant which represents the maximum inelastic strain rate, Z_0 is a material constant which represented the initial, isotropic "hardness" of the material before any load is applied, n is a material constant which controls the rate dependence of the deformation response and K_2 is defined as follows:

$$K_2 = \tfrac{1}{2}(s_{ij}-\Omega_{ij})(s_{ij}-\Omega_{ij}) \tag{2}$$

This flow equation is identical to that used in the original model, except for the fact that in the original model the isotropic hardness variable Z can vary as cyclic loads are applied. For the current application, cyclic loading is not considered to be significant, so the value of Z was assumed to be constant (Z_0). The elastic components of strain are added to the inelastic strain to obtain the total strain.

The following relation defines the internal stress variable rate:

$$\dot{\Omega}_{ij} = \tfrac{2}{3}q\Omega_m\dot{\varepsilon}_{ij}^{I} - q\Omega_{ij}\dot{\varepsilon}_{e}^{I} \tag{3}$$

where q is a material constant that represents the "hardening" rate, Ω_m is a material constant that represents the maximum value of the internal stress, and $\dot{\varepsilon}_{e}^{I}$ is the effective

inelastic strain rate, defined as follows:

$$\dot{\varepsilon}_e^I = \sqrt{\tfrac{2}{3}\dot{\varepsilon}_{ij}^I \dot{\varepsilon}_{ij}^I} \tag{4}$$

The internal stress is assumed to be equal to zero when the material is in its virgin state. The internal stress evolution equation in the original Ramaswamy–Stouffer equation is as follows:

$$\dot{\Omega}_{ij} = \tfrac{2}{3} f_1 \dot{\varepsilon}_{ij}^I - f_1 \frac{\Omega_{ij}}{\Omega_m} \dot{\varepsilon}_e^I + f_2 \dot{s}_{ij} \tag{5}$$

where f_1 and f_2 are material constants, and the remaining terms are as defined earlier. By comparing Equations (3) and (5), one can observe that the relationships are quite similar. The modifications made to the equation include setting the new constant q equal to the product of the old constants f_1 and Ω_m, and the additional term in the original equation related to the stress rate is not used. In the original equations, this additional term was required in order to increase the hardening at low strains in the tensile loading of metals. Such a correction was found not to be required for the polymers considered here.

The values of the material constants are determined using the following procedure. First, Equations (1) and (2) are simplified for the case of uniaxial loading, resulting in the following expressions:

$$\dot{\varepsilon}^I = \frac{2}{\sqrt{3}} D_0 \exp\left[-\frac{1}{2}\left(\frac{Z_0}{|\sigma - \Omega|} \right)^{2n} \right] \frac{\sigma - \Omega}{|\sigma - \Omega|} \tag{6}$$

$$\dot{\Omega} = q\Omega_m \dot{\varepsilon}^I - q\Omega |\dot{\sigma}^I| \tag{7}$$

where $\dot{\varepsilon}^I$ is the uniaxial inelastic strain rate, σ is the uniaxial stress, and Ω is the uniaxial value of the internal stress. D_0 is assumed to be equal to a value 10^4 times the maximum applied total strain rate, and is considered to be the limiting value of the inelastic strain rate.

The values of n, Z_0 and Ω_m are determined as follows. First, the natural logarithm of both sides of Equation (6) is taken. The values of the inelastic strain rate, stress, and state variable Ω at saturation are substituted into the resulting expression, resulting in the following equation:

$$\ln\left[-2\ln\left(\frac{\sqrt{3}\dot{\varepsilon}_0}{2D_0} \right) \right] = 2n\ln(Z_0) - 2n\ln(\sigma_s - \Omega_m) \tag{8}$$

where σ_s equals the saturation stress, $\dot{\varepsilon}_0$ is the constant applied total strain rate, and the remaining terms are as defined earlier.

The required constants are determined from a set of tensile curves obtained from constant strain rate tests. Each curve in this set is obtained at a different constant strain rate. Data pairs of the total strain rate and saturation stress values from each curve are taken. Values for Ω_m are estimated for the material, with initial estimates ranging from 50 to 75% of the highest saturation stress found to work well. These estimates

are similar to the values used for large-grain metals. For each strain rate, the data values are substituted into Equation (8), and represent a point on a master curve. The number of points in the master curve equal the number of strain rates at which tensile tests were conducted. A least squares regression analysis is then performed on the master curve. As suggested by Equation (8), the slope of the best fit line is equal to $-2n$. The intercept of the best fit line is equal to $2n\ln(Z_0)$. The value for Ω_m is then adjusted until an optimal fit to the data is obtained.

To determine the value for q, Equation (7) is utilized. At saturation, the value of the internal stress is assumed to approach the maximum value, resulting in the exponential term approaching zero. Assuming that saturation occurs when the following condition is satisfied:

$$\exp(-q\varepsilon_s^I) = 0.01 \tag{9}$$

the equation is solved for q, where ε_s^I is the inelastic strain at saturation. If the inelastic strain at saturation is found to vary with strain rate, the parameter q is computed at each strain rate and regression techniques are utilized to determine an expression for the variation of q. Further information on the determination of the material constants can be found in Stouffer and Dame [18] and Goldberg [23].

The hydrostatic stress state has been found to have a significant effect on the yield behavior of a polymer [17]. Bordonaro [22] indicated a possible way of accounting for such effects in a state variable constitutive model was to modify the effective stress terms. In this work, pressure dependence is included by multiplying the shear terms in the K_2 invariant in Equation (2) by the following correction factor:

$$\alpha = \left(\frac{\sigma_m}{\sqrt{J_2}}\right)^{\beta} \tag{10}$$

In this term, σ_m is the mean stress, J_2 is the second invariant of the deviatoric stress tensor, and β is a material constant. Since only uniaxial data were available for the polymers that are considered in this study, the value of the parameter β was determined empirically by fitting data from uniaxial composites with shear dominated fiber orientation angles, such as [15°]. Future efforts will concentrate on developing more systematic methods of determining the value of β.

Numerical Implementation of Constitutive Equations

To test and correlate the constitutive equations, a stand-alone computer code has been developed. To integrate the flow and evolution laws, the standard fourth order Runge-Kutta explicit integration routine is used [24]. For this class of equations, implicit integration routines have often been used because of their inherent numerical stability [18]. However, to be able to use the equations in impact studies, the equations will need to be implemented into a transient dynamic finite element code, which uses explicit integration schemes. Therefore, in developing the stand-alone computer code, an explicit integration scheme is used in order to facilitate the eventual finite element implementation. The Runge-Kutta method is employed for this study due to its simplicity and ease of

implementation. Future efforts might include investigating more robust numerical techniques such as semi-implicit algorithms, which provide the stability of implicit methods while still maintaining the appearance of an explicit technique.

To compute the value of a set of variables y_n at time step $t + \Delta t$, where t is the current time and Δt is the time increment, the following equations are used:

$$y_n(t + \Delta t) = y_n(t) + \tfrac{1}{6}(k_1 + 2k_2 + 2k_3 + k_4) \tag{11}$$

$$k_1 = \Delta t\, y_n'(t,\, y_n) \tag{12}$$

$$k_2 = \Delta t\, y_n'\left(t + \tfrac{1}{2}\Delta t,\, y_n + \tfrac{1}{2}k_1\right) \tag{13}$$

$$k_3 = \Delta t\, y_n'\left(t + \tfrac{1}{2}\Delta t,\, y_n + \tfrac{1}{2}k_2\right) \tag{14}$$

$$k_4 = \Delta t\, y_n'(t + \Delta t,\, y_n + k_3) \tag{15}$$

where y_n' is the time derivative of variable y_n.

For the stand-alone code developed to correlate and test the constitutive equations, strain controlled loading is assumed. This condition is applied for two reasons. First, in a finite element application, strains and/or strain increments are passed from the main code into a user developed material subroutine. The routine then computes the stresses based on the supplied strains. Similar conditions are assumed here to facilitate finite element implementations. Second, the tensile tests that are used to correlate the model were conducted at constant strain rate. Utilizing strain controlled loading in the stand-alone computer code simplifies the simulation of these tests.

To determine the value of the total strain, inelastic strain, and internal stress at time $t + \Delta t$, where t is the current time and Δt is the time increment, the following algorithm is utilized for each step of the Runge-Kutta integration. The strains at time t (or strain estimates at time $t + 0.5\Delta t$) are passed into the integration routine. The stresses are computed using the elastic constants and the current value of the inelastic strains. The effective stress K_2 is then computed using Equation (2). The inelastic strain rate is computed using Equation (1), and the internal stress rate is computed using Equations (3) and (4). The elastic Poisson's ratio and the inelastic strain rates are then used to compute the total strain rates. The total strain, inelastic strain and internal stress are computed by integrating the corresponding rate equations using Equations (11)–(15).

Model Correlation Studies

To demonstrate the usefulness of this model, a PEEK (polyetheretherketone) thermoplastic matrix is characterized and modeled based on uniaxial tensile data found in [22] for strain rates ranging from 1×10^{-6} to 11×10^{-3}/s. The goal of this research is to model high strain-rate impact problems. However, at the time of the writing of this report, suitable high strain rate data was not available, so only low rate analyses were conducted. High strain rate data for a representative toughened epoxy and a polymer matrix

composite using the toughened epoxy are currently being obtained. A future report will describe the high strain rate testing and analysis of this material. The analyses should show that the constitutive model works for a variety of ductile polymers.

For the PEEK material at the strain rates examined, all of the constants have been found to be rate independent. As mentioned above, the constants D_0, n, Z_0, and Ω_m are determined using data from a variety of strain rates. If high strain rate data would be available, while the values of these constants might vary somewhat due to the nature of curve fitting, in an ideal case the constants determined from low rate tests should be identical to those determined using both low and high rate data. For this particular material and range of strain rates examined, the constants q and β were found to be strain rate independent. However, for different materials and/or higher strain rates, these constants might be found to be strain rate dependent and would need to be determined for each strain rate. A regression equation could then be developed to model the value of these constants as a function of strain rate. For the PEEK material, the elastic modulus of the material is 4000 MPa and the Poisson's ratio is 0.40. The inelastic material constants were determined to be as follows using the procedures described above: $D_0 = 1 \times 10^4$/s, $n = 0.70$, $Z_0 = 630$ MPa, $q = 310$, $\Omega_m = 52$ MPa, $\beta = 0.40$.

Experimental [22] and computed results for the bulk PEEK material at strain rates of 1×10^{-6} and 1×10^{-3}/s are shown in Figure 1. Composite data will be shown in later figures. As can be seen in the figure, there is an excellent correlation between the experimental and predicted results. Note that while the tensile data is used to obtain the material constants, the constants are not explicitly modified in order to improve the fit of the computed results to the experimental data. These results indicate that the constitutive equations described here can do a good job in computing the rate dependent deformation response of a ductile polymer.

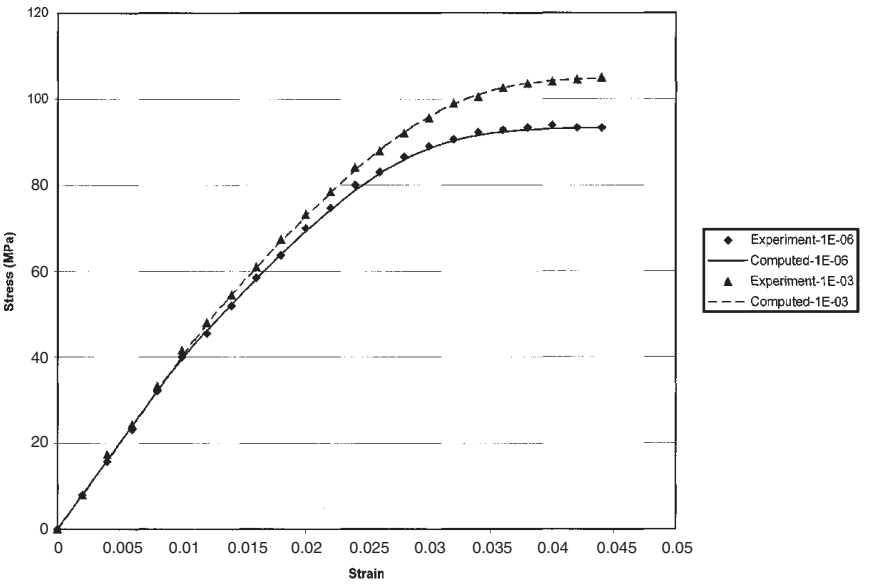

Figure 1. *Model correlations of PEEK thermoplastic at strain rates of 1×10^{-6}/s (1E-06) and 1×10^{-3}/s (1E-03).*

COMPOSITE MICROMECHANICAL MODEL

Overview and Assumptions

Micromechanics techniques are used to predict the effective properties and deformation response of the polymer matrix composites examined in this study. In micromechanics, the effective properties and response are computed based on the properties of the individual constituents. The common procedure is to analyze a unit cell of the composite, the smallest material unit for which the response can be considered representative of the response of the overall composite.

For this study, the composite unit cell is defined as consisting of a single continuous fiber and its surrounding matrix. Only unidirectional composites at various fiber orientation angles are analyzed. Laminate theory is currently being implemented into the micromechanics, and adding the capability to model woven composites will be considered at a later time. The composites are also assumed to have a periodic, square fiber packing with a perfect interfacial bond, which are common assumptions in micromechanical analysis techniques [7,9]. Small strain conditions are assumed, and temperature effects are once again neglected. The fibers are assumed to be transversely isotropic and linearly elastic. The matrix is assumed to be isotropic, with a rate dependent, nonlinear deformation response computed using the constitutive equations described in the previous section.

The micromechanics method utilized in this study is similar to and based on the approach originally proposed by Sun and Chen [25] and extended by Robertson and Mall [26]. The methodology is also similar to that derived by Pindera and Bednarcyk in their reformulation of the Generalized Method of Cells [27]. Pecknold and Rahman [28] also used a similar model. In their model, a three region unit cell model was used with appropriate uniform stress and uniform strain assumptions applied to the model. A nonlinear elastic constitutive model was applied to simulate the nonlinear deformation response of the matrix. For this study, the composite unit cell is broken up into four rectangular subregions, where the fiber is idealized as having a square shape, as shown in Figure 2. Note that in [25] and [26] the analysis model shown was assumed to be one-quarter of the unit cell with symmetry applied. Pindera and Bednarcyk [27] assumed that the analysis model could represent the entire unit cell. For the case of periodic, square fiber packing, both assumptions on the analysis cell geometry yield identical micromechanics equations. In the unit cell, subregion "A_f" represents the fiber and subregions "$M1$", "$M2$" and "$M3$" are composed of matrix material. The bottom layer of subregions ("A_f" and "$M1$") is referred to as Row 1 ($R1$), and the top layer of subregions ("$M2$" and "$M3$") is referred to as Row 2 ($R2$). Likewise, Column 1 ($C1$) is defined as consisting of subregions "A_f" and "$M2$", and Column 2 ($C2$) is defined as consisting of subregions "$M1$" and "$M3$". In the material axis system shown in the figure, the "1" coordinate direction is along the fiber direction, the "2" coordinate direction is perpendicular to the fiber in the plane of the composite, and the "3" coordinate direction is perpendicular to the fiber in the out of plane direction.

In the micromechanics equations used in this study, strain controlled loading is assumed, and the total strains in the unit cell in the material axis system as well as the inelastic strains in each subregion of the unit cell are considered to be known. In the actual computer algorithm used to compute the composite deformation response, the strains are specified in a particular structural axis direction. The Poisson and axial-shear coupling

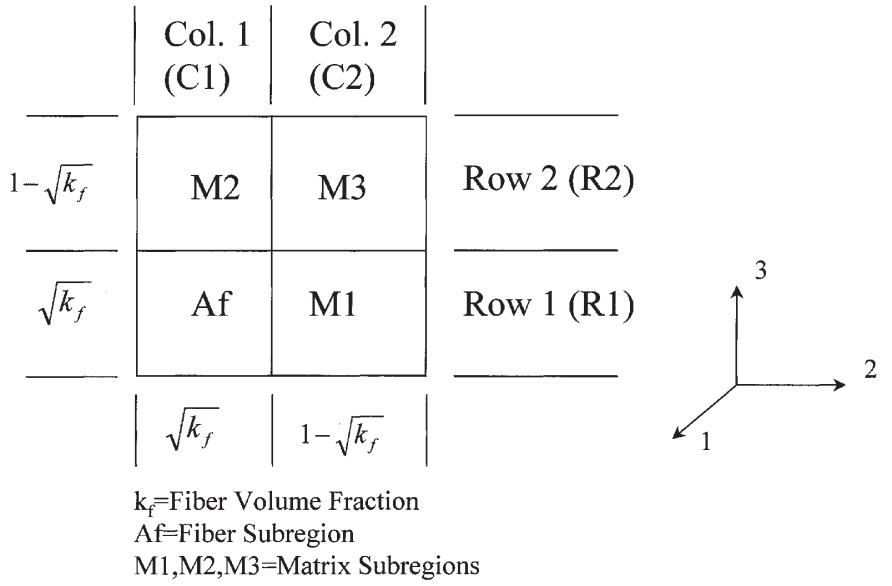

Figure 2. *Geometry and layout of unit cell model.*

strains in both the structural and material axis systems are determined using effective elastic constants calculated using the micromechanics equations and standard coordinate transformation techniques [7–9].

Derivation of Micromechanics Equations

In the following equations, the subscript "f" is used to denote fiber related properties, and the subscript "m" is used to denote matrix related properties. Subscripts "A_f", "$M1$", "$M2$", "$M3$", "$R1$", "$R2$", "$C1$" and "$C2$" are used to denote stresses and strains in the appropriate region or subregion of the unit cell. Stresses and strains with no region identifying subscript are assumed to represent the total effective stresses and strains for the unit cell. A superscript "I" is used to denote inelastic strains. The subscripts "11", "22" and "33" are used to denote stresses, strains and material properties along the coordinate axes, while the subscript "12" is used to denote in-plane shear stresses, strains, and material properties. Out of plane shear stresses and strains are neglected in the current analyses. However, these effects could be incorporated into the analyses using similar methods to those presented below. The symbol σ_{ij} represents stress tensor components, the symbol ε_{ij} represents strain tensor components, and the symbol γ_{ij} represents engineering shear strain components, all assigned in a Cartesian frame of reference. The symbol v_f represents the fiber volume ratio of the composite.

The stress and strain in each subregion are assumed to be the effective stress and strain, equal to the average stress or strain over the volume of the subregion, and are assumed to be uniform over the volume of the subregion. The effective stress and strain in Row 1, Row 2, Column 1 and Column 2 are defined as the volume average of the stresses and strains in the component subregions. The effective stress and strain in the unit cell are defined as the volume average of the stresses and strains in Row 1 and Row 2 (or Column 1

and Column 2). To determine the volume average, a weighted sum is computed where the value (stress or strain) in each subregion or combination of subregions is weighted by the volume ratio of the subregion or combination of subregions.

The transversely isotropic compliance matrix is used to relate the strains to the stresses, using the following relations. Note that in these equations S_{ij} represents the components of the compliance matrix, not the components of the deviatoric stress tensor s_{ij} as in the previous section.

$$\begin{Bmatrix} \varepsilon_{11} \\ \varepsilon_{22} \\ \varepsilon_{33} \end{Bmatrix} = \begin{bmatrix} S_{11} & S_{12} & S_{12} \\ S_{12} & S_{22} & S_{23} \\ S_{12} & S_{23} & S_{22} \end{bmatrix} \begin{Bmatrix} \sigma_{11} \\ \sigma_{22} \\ \sigma_{33} \end{Bmatrix} + \begin{Bmatrix} \varepsilon_{11}^I \\ \varepsilon_{22}^I \\ \varepsilon_{33}^I \end{Bmatrix} \tag{16}$$

$$\gamma_{12} = S_{66}\sigma_{12} + 2\varepsilon_{12}^I \tag{17}$$

The addition of the inelastic strain components to the standard transversely isotropic elastic constitutive law facilitates the incorporation of inelasticity into the constitutive relations. For the fiber, which is assumed to be linear elastic, these components are neglected. For the matrix material, which is assumed to be isotropic, S_{23} is set equal to S_{12} and S_{22} is set equal to S_{11}.

For the normal stresses and strains (11, 22 and 33), the following uniform stress and uniform strain assumptions are made:

In the fiber direction:

$$\varepsilon_{11A_f} = \varepsilon_{11M1} = \varepsilon_{11R1} = \varepsilon_{11M2} = \varepsilon_{11M3} = \varepsilon_{11R2} = \varepsilon_{11} \tag{18}$$

Normal to the fiber, in the plane of the ply:

$$\begin{aligned} \sigma_{22A_f} &= \sigma_{22M1} = \sigma_{22R1} \\ \sigma_{22M2} &= \sigma_{22M3} = \sigma_{22R2} \end{aligned} \tag{19}$$

$$\varepsilon_{22R1} = \varepsilon_{22R2} = \varepsilon_{22} \tag{20}$$

Normal to the fiber, normal to the plane of the ply:

$$\begin{aligned} \sigma_{33A_f} &= \sigma_{33M2} = \sigma_{33C1} \\ \sigma_{33M1} &= \sigma_{33M3} = \sigma_{33C2} \end{aligned} \tag{21}$$

$$\varepsilon_{33C1} = \varepsilon_{33C2} = \varepsilon_{33} \tag{22}$$

The effective stresses and strains in Row 1, Row 2, Column 1 and Column 2, as well as for the composite unit cell, are computed using volume averaging, yielding the following expressions:

$$\varepsilon_{22R1} = \sqrt{v_f}\varepsilon_{22A_f} + (1 - \sqrt{v_f})\varepsilon_{22M1} \tag{23}$$

$$\varepsilon_{22R2} = \sqrt{v_f}\varepsilon_{22M2} + (1 - \sqrt{v_f})\varepsilon_{22M3} \tag{24}$$

$$\varepsilon_{33C1} = \sqrt{v_f}\varepsilon_{33A_f} + (1 - \sqrt{v_f})\varepsilon_{33M2} \tag{25}$$

$$\varepsilon_{33C2} = \sqrt{v_f}\varepsilon_{33M1} + (1 - \sqrt{v_f})\varepsilon_{33M3} \tag{26}$$

$$\sigma_{11R1} = \sqrt{v_f}\sigma_{11A_f} + (1 - \sqrt{v_f})\sigma_{11M1} \tag{27}$$

$$\sigma_{11R2} = \sqrt{v_f}\sigma_{11M2} + (1 - \sqrt{v_f})\sigma_{11M3} \tag{28}$$

$$\sigma_{11} = \sqrt{v_f}\sigma_{11R1} + (1 - \sqrt{v_f})\sigma_{11R2} \tag{29}$$

$$\sigma_{22} = \sqrt{v_f}\sigma_{22R1} + (1 - \sqrt{v_f})\sigma_{22R2} \tag{30}$$

$$\sigma_{33} = \sqrt{v_f}\sigma_{33C1} + (1 - \sqrt{v_f})\sigma_{33C2} \tag{31}$$

By applying the constitutive relations [Equation (16)] for each subregion, and by utilizing the appropriate uniform stress and uniform strain assumptions, the following expressions are obtained.

$$\sigma_{11A_f} = \frac{1}{S_{11f}}(\varepsilon_{11} - S_{12f}\sigma_{22R1} - S_{12f}\sigma_{33C1}) \tag{32}$$

$$\sigma_{11M1} = \frac{1}{S_{11m}}(\varepsilon_{11} - S_{12m}\sigma_{22R1} - S_{12m}\sigma_{33C2} - \varepsilon^I_{11M1}) \tag{33}$$

$$\sigma_{11M2} = \frac{1}{S_{11m}}(\varepsilon_{11} - S_{12m}\sigma_{22R2} - S_{12m}\sigma_{33C1} - \varepsilon^I_{11M2}) \tag{34}$$

$$\sigma_{11M3} = \frac{1}{S_{11m}}(\varepsilon_{11} - S_{12m}\sigma_{22R2} - S_{12m}\sigma_{33C2} - \varepsilon^I_{11M3}) \tag{35}$$

$$\begin{aligned}
&\varepsilon_{22} - \left(\sqrt{v_f}\frac{S_{12f}}{S_{11f}} + (1 - \sqrt{v_f})\frac{S_{12m}}{S_{11m}}\right)\varepsilon_{11} + (1 - \sqrt{v_f})\frac{S_{12m}}{S_{11m}}\varepsilon^I_{11M1} - (1 - \sqrt{v_f})\varepsilon^I_{22M1} \\
&\quad = \left(\sqrt{v_f}\left(S_{22f} - \frac{S^2_{12f}}{S_{11f}}\right) + (1 - \sqrt{v_f})\left(S_{11m} - \frac{S^2_{12m}}{S_{11m}}\right)\right)\sigma_{22R1} \\
&\qquad + \left(\sqrt{v_f}\left(S_{23f} - \frac{S^2_{12f}}{S_{11f}}\right)\right)\sigma_{33C1} + \left((1 - \sqrt{v_f})\left(S_{12m} - \frac{S^2_{12m}}{S_{11m}}\right)\right)\sigma_{33C2}
\end{aligned} \tag{36}$$

$$\begin{aligned}
&\varepsilon_{22} - \frac{S_{12m}}{S_{11m}}\varepsilon_{11} + \sqrt{v_f}\frac{S_{12m}}{S_{11m}}\varepsilon^I_{11M2} - \sqrt{v_f}\varepsilon^I_{22M2} + (1 - \sqrt{v_f})\frac{S_{12m}}{S_{11m}}\varepsilon^I_{11M3} - (1 - \sqrt{v_f})\,\varepsilon^I_{22M3} \\
&\quad = \left(S_{11m} - \frac{S^2_{12m}}{S_{11m}}\right)\sigma_{22R2} + \left(\sqrt{v_f}\left(S_{12m} - \frac{S^2_{12m}}{S_{11m}}\right)\right)\sigma_{33C1} \\
&\qquad + \left((1 - \sqrt{v_f})\left(S_{12m} - \frac{S^2_{12m}}{S_{11m}}\right)\right)\sigma_{33C2}
\end{aligned} \tag{37}$$

$$\varepsilon_{33} - \left(\sqrt{v_f}\frac{S_{12f}}{S_{11f}} + (1-\sqrt{v_f})\frac{S_{12m}}{S_{11m}}\right)\varepsilon_{11} + (1-\sqrt{v_f})\frac{S_{12m}}{S_{11m}}\varepsilon^I_{11M2} - (1-\sqrt{v_f})\varepsilon^I_{33M2}$$
$$= \left(\sqrt{v_f}\left(S_{22f} - \frac{S^2_{12f}}{S_{11f}}\right) + (1-\sqrt{v_f})\left(S_{11m} - \frac{S^2_{12m}}{S_{11m}}\right)\right)\sigma_{33C1}$$
$$+ \left(\sqrt{v_f}\left(S_{23f} - \frac{S^2_{12f}}{S_{11f}}\right)\right)\sigma_{22R1} + \left((1-\sqrt{v_f})\left(S_{12m} - \frac{S^m_{12m}}{S_{11m}}\right)\right)\sigma_{22R2} \tag{38}$$

$$\varepsilon_{33} - \frac{S_{12m}}{S_{11m}}\varepsilon_{11} + \sqrt{v_f}\frac{S_{12m}}{S_{11m}}\varepsilon^I_{11M1} - \sqrt{v_f}\varepsilon^I_{33M1} + (1-\sqrt{v_f})\frac{S_{12m}}{S_{11m}}\varepsilon^I_{11M3} - (1-\sqrt{v_f})\varepsilon^I_{33M3}$$
$$= \left(S_{11m} - \frac{S^2_{12m}}{S_{11m}}\right)\sigma_{33C2} + \left(\sqrt{v_f}\left(S_{12m} - \frac{S^2_{12m}}{S_{11m}}\right)\right)\sigma_{22R1}$$
$$+ \left((1-\sqrt{v_f})\left(S_{12m} - \frac{S^2_{12m}}{S_{11m}}\right)\right)\sigma_{22R2} \tag{39}$$

Equations (36)–(39) form a system of equations that can be solved for the required subregion normal stresses σ_{22R1}, σ_{22R2}, σ_{33C1} and σ_{33C2}. These values are substituted into Equations (32)–(35), which are then applied to solve for the remaining subregion normal stresses. Equations (19), (21), and (27)–(31) are then used to compute the effective total stresses in the unit cell. From these results, the effective normal inelastic strains for the unit cell are also computed.

For the in-plane shear (1–2 direction) stresses and strains, the following uniform stress and uniform strain assumptions are made:

$$\gamma_{12R1} = \gamma_{12R2} = \gamma_{12} \tag{40}$$

$$\sigma_{12A_f} = \sigma_{12M1} = \sigma_{12R1}$$
$$\sigma_{12M2} = \sigma_{12M3} = \sigma_{12R2} \tag{41}$$

By applying volume averaging, the effective in-plane shear stresses and strains for Row 1, Row 2, and the composite unit cell are defined as follows:

$$\gamma_{12R1} = \sqrt{v_f}\gamma_{12A_f} + (1-\sqrt{v_f})\gamma_{12M1}$$
$$\gamma_{12R2} = \sqrt{v_f}\gamma_{12M2} + (1-\sqrt{v_f})\gamma_{12M1} \tag{42}$$

$$\sigma_{12} = \sqrt{v_f}\sigma_{12R1} + (1-\sqrt{v_f})\sigma_{12R2} \tag{43}$$

By using Equation (17) and the appropriate uniform stress and uniform strain assumptions, the following expressions are obtained, from which the subregion in-plane shear stresses are computed. From these expressions, the effective inelastic in-plane shear strain can also be determined.

$$\gamma_{12} = \left[\sqrt{v_f}S_{66f} + (1-\sqrt{v_f})S_{66m}\right]\sigma_{12R1} + 2(1-\sqrt{v_f})\varepsilon^I_{12M1} \tag{44}$$

$$\gamma_{12} = S_{66m}\sigma_{12R2} + 2\sqrt{v_f}\varepsilon^I_{12M2} + 2(1-\sqrt{v_f})\varepsilon^I_{12M3} \tag{45}$$

Numerical Implementation of Micromechanics Equations

For the current study, a stand-alone computer code has been developed in order to implement and test the micromechanics equations. A standard fourth order Runge-Kutta explicit integration scheme is again utilized to integrate the rate dependent constitutive equations. The details of the method are as described earlier.

As mentioned in the development of the micromechanics equations, strain controlled loading is assumed in the formulation. In the computer algorithm, strains are specified in a particular coordinate direction. To impose the required Poisson and axial-shear coupling strains, effective elastic properties for the composite at a specified fiber orientation angle are utilized. First, the elastic constants in the material axis system are computed using the basic micromechanics equations. The elastic constants in the structural axis system are then computed using standard techniques and equations described in [7–9]. The material axis system is the coordinate system shown in Figure 2. The structural axis system is the axis system along which the loads are applied. The material coordinate system is obtained by rotating the structural axis system about the "3" coordinate axis by an amount equal to the fiber orientation angle.

For the computer code execution, first the required geometric data (fiber volume ratio and fiber orientation angle), constituent properties and load history data are read in from an input file. The required elastic constants in both material and structural coordinate systems are computed, along with the required tensor transformation matrices. For each time step, the total strain rate in the load direction is determined. The Runge-Kutta integration procedure is then carried out to compute the total strains in the structural axis system, as well as the inelastic strains and internal stresses in each subregion. The total stresses in structural coordinates are calculated using the total strains, appropriate tensor transformations, and the micromechanics equations. At this point, the code moves on to the next time step.

The Runge-Kutta integration algorithm involves the computation of several intermediate estimates of the total strains, subregion inelastic strains and subregion internal stresses. To calculate the intermediate estimates, first the total strain estimates are converted from the structural axis system to the material axis system. The stresses in each of the subregions are then determined using the micromechanics equations and the current value of the inelastic strain estimates. Using the computed stresses, the inelastic strain rates and internal stress rates in each matrix subregion are computed using the polymer constitutive equations [Equations (1–4)]. The effective inelastic strain rate tensor for the composite unit cell in the material axis system is computed, and the values are then transformed into the structural axis system. Using the ply level Poisson's ratios and axial-shear coupling coefficients, the total strain rate tensor in structural coordinates is calculated. The intermediate values required for the Runge-Kutta integration routine are then determined.

Verification Studies

To verify the micromechanics equations, a series of analyzes have been carried out on a composite composed of carbon AS-4 fibers in a PEEK thermoplastic matrix. Tensile stress–strain curves were obtained by Weeks and Sun [4] for unidirectional composites with various fiber orientations at strain rates of 1×10^{-5}, and 0.1/s. Only low strain rate

data are examined since the PEEK material has only been characterized for relatively low strain rates. Furthermore, only uniaxial test data were available. While modeling tension–torsion or biaxial tension tests might more fully exercise the model, such data were not available. However, since in the matrix subregions a full three-dimensional stress state exists, the ability of the polymer constitutive equations to model the full three-dimensional behavior of the matrix can be determined to some extent, at least within the realm of the composite micromechanics.

The fiber volume ratio used for the AS4/PEEK material is 0.62 (a typical value for this material based on representative manufacturer information). The elastic properties of the AS-4 fibers include a longitudinal elastic modulus of 214 GPa, transverse and in-plane shear moduli of 14 GPa, a longitudinal Poisson's ratio of 0.20 and a transverse Poisson's ratio of 0.25 [29]. For the PEEK matrix, the material properties are as described in the previous section on the polymer constitutive model.

Experimental and predicted stress–strain curves at both strain rates are shown in Figures 3–5 for composites with fiber orientations of [15°], [30°] and [45°], respectively. As can be seen in the figures, for all of the fiber orientations the results computed using the micromechanics equations compare favorably to the experimental results for both strain rates. In particular, the nonlinearity and rate dependence observed in the experimental curves are captured by the micromechanics predictions. The stresses in the elastic range are somewhat underpredicted, indicating that the shear modulus or transverse Poisson's ratio of the fiber may not be correct. A point to note is that in Figure 3 the experimental and predicted elastic moduli for the two strain rates are slightly different. This discrepancy is due to the fact that for the lower strain rate, the composite actually has a fiber orientation angle of [14°], which results in a slightly different elastic modulus than for the case where the composite has a [15°] fiber orientation.

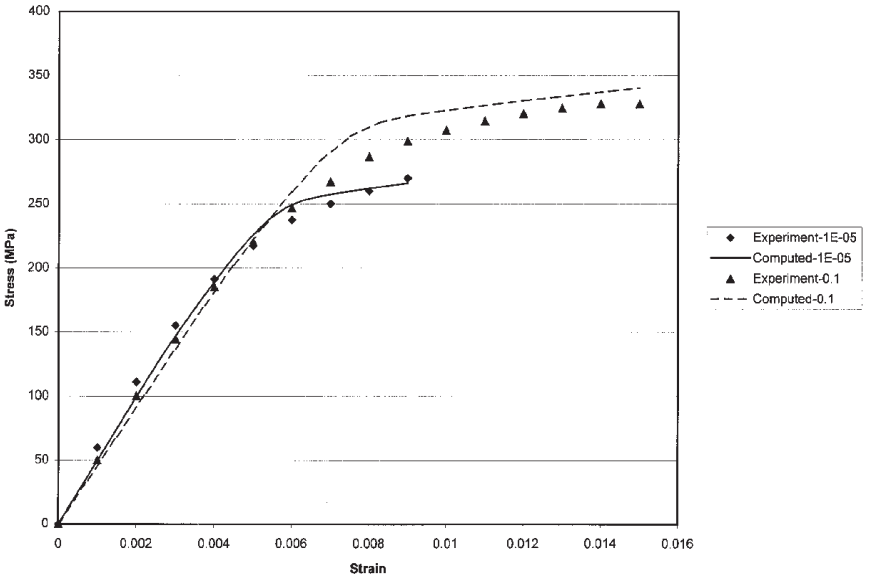

Figure 3. *Model predictions for AS4/PEEK [15°] laminate at strain rates of 1×10^{-5}/s (1E-05) and 0.1/s.*

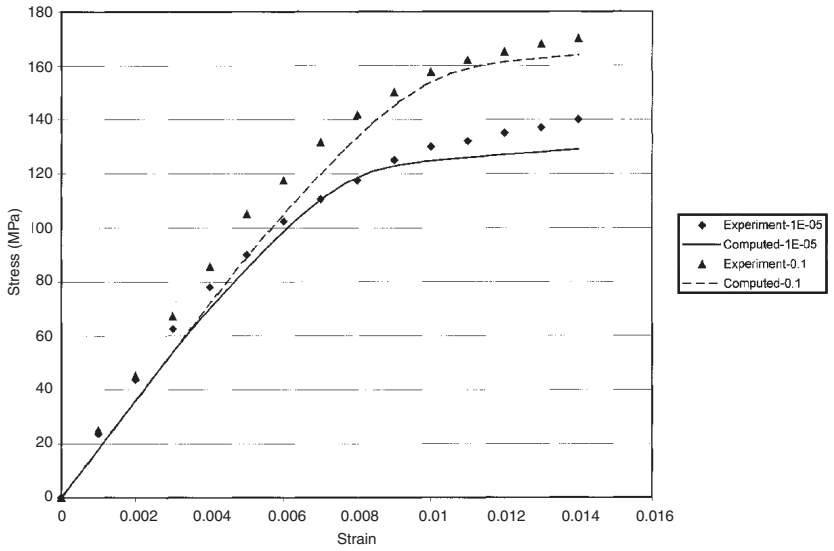

Figure 4. *Model predictions for AS4/PEEK [30°] laminate at strain rates of 1×10^{-5}/s (1E-05) and 0.1/s.*

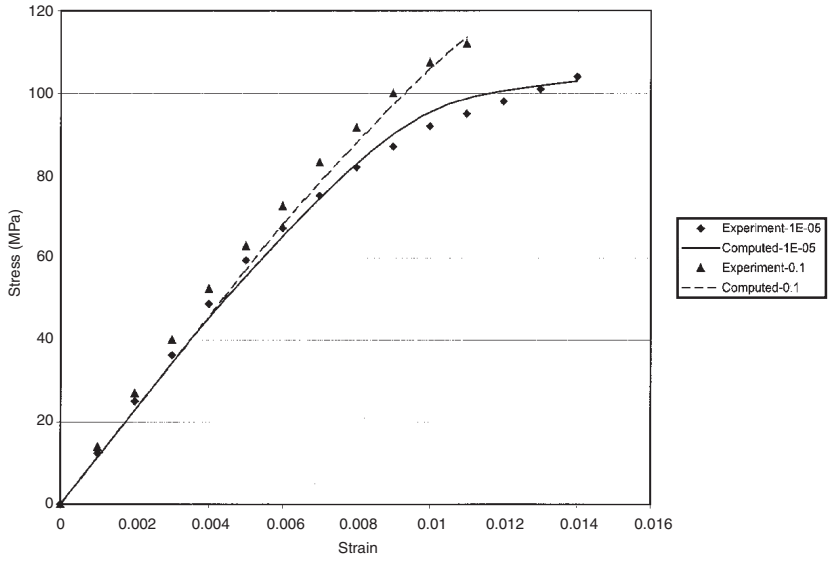

Figure 5. *Model predictions for AS4/PEEK [45°] laminate at strain rates of 1×10^{-5}/s (1E-05) and 0.1/s.*

PLY STRENGTH PREDICTIONS

In order to predict the rate dependent ultimate strength of a composite ply, a failure model has been implemented into the composite micromechanics equations. This capability is required in order to allow for the future development of structural level penetration and failure models that can be applied to high strain rate impact applications. For this study, the Hashin failure model [10] has been chosen due to its ability to predict

the occurrence of local failure mechanisms (such as fiber failure or matrix cracking) using macroscopic (ply level) stresses and strengths. Traditional failure criterion such as the Tsai–Wu criterion might be easier to implement, particularly since only one equation would be required. However, use of such an equation would make the development of property degradation models more difficult, since specific failure modes could not be identified. Furthermore, as discussed in the introduction failure models such as the Hashin model have been frequently used in the study of impact in composites, the ultimate goal of this research. Another important point to note is that eventhough constituent level stresses are computed in the micromechanics equations, ply level strength data were more readily available and considered to be more reliable than constituent level strength data for the materials considered in this study.

Several approximations are utilized in the implementation of the failure models. Since only in-plane loads are considered in this study and the out of plane stresses are reasonably small, the plane stress versions of the criteria are employed. However, in the future study of impact problems, where out of plane stresses would be significant, the full three-dimensional version of the criteria will be used. For the purposes of this study, once any of the failure criteria are violated, property degradation is neglected, and total composite failure is assumed to have occurred.

Failure criteria for each of the local failure modes are as follows. In each of the expressions, σ_{ij} is the macroscopic stress component, X_T is the ply tensile strength in the longitudinal (fiber) direction, and X_C is the compressive strength in the longitudinal direction. Furthermore, Y_T is the tensile strength in the transverse direction (perpendicular to the fiber in the plane of the composite), Y_C is the compressive strength in the transverse direction, and X_S is the ply in-plane shear strength. Failure is assumed to occur when the value of the strength expression becomes greater than or equal to one [1]. Tensile fiber failure is predicted by using the following expression:

$$\left(\frac{\sigma_{11}}{X_T}\right)^2+\left(\frac{\sigma_{12}}{X_S}\right)^2=1 \tag{46}$$

Compressive fiber failure is predicted using the following equation. Shear stresses are not included in the failure criterion since Hashin was unsure whether shear stresses increased or decreased the compressive strength. Therefore, the effects of shear stresses are neglected [10]. Note that local effects such as microbuckling are not explicitly accounted for in the failure criterion.

$$\frac{|\sigma_{11}|}{X_C}=1 \tag{47}$$

Tensile matrix failure is predicted using the following expression:

$$\left(\frac{\sigma_{22}}{Y_T}\right)^2+\left(\frac{\sigma_{12}}{X_S}\right)^2=1 \tag{48}$$

Compressive matrix failure is predicted as follows:

$$\left(\frac{\sigma_{22}}{2X_S}\right)^2+\left[\left(\frac{Y_C}{2X_S}\right)^2-1\right]\frac{\sigma_{22}}{Y_C}+\left(\frac{\sigma_{12}}{X_S}\right)^2=1 \tag{49}$$

The ply strengths of the AS4/PEEK material considered earlier have been predicted. For the AS4/PEEK material, the longitudinal tensile strength is set to 2070 MPa, and the transverse tensile strength is set to 83 MPa [30]. These values have been determined to be strain rate independent for this material. As mentioned in the introduction, the longitudinal tensile strength of carbon fiber reinforced composites has been found to be independent of strain rate by a variety of researchers (e.g. [1–3]). For this material, the transverse modulus has been found to be strain rate independent [4], leading to the assumption that the transverse tensile strength is most likely also strain rate independent. The longitudinal compressive strength is set equal to 1080 MPa, and the transverse compressive strength is set equal to 196 MPa [8]. The in-plane shear strength is assumed to be rate dependent, and has been correlated based on data from [15°] off-axis laminates found in [4]. This orientation has been chosen since it is a shear dominated fiber orientation angle. From this data, the shear strength for a strain rate of 1×10^{-5}/s is determined to be 63 MPa, and the shear strength for a strain rate of 0.1/s is determined to be 85 MPa. The strength values and the experimental values for the failure stresses shown below likely have some scatter, but the statistical data were not available.

Using the given strength values, failure stresses have been predicted for [30°] and [45°] laminates for strain rates of 1×10^{-5} and 0.1/s. The predicted and experimental [4] ultimate tensile strengths and failure strains for a strain rate of 1×10^{-5}/s are shown in Table 1, and the results for a strain rate of 0.1/s are shown in Table 2. In all cases, failure is predicted to be due to tensile matrix failure.

For both strain rates and for both fiber orientations examined, the comparison between the predicted and experimental strength values is quite good and most likely within the experimental scatter. For the [30°] laminate the failure strain is somewhat overpredicted. For the [45°] laminate the failure strain is predicted reasonably well. Presumably if the deformation model could be revised such that the predicted stresses for the [30°] laminate would increase (and become closer to the experimental results) the failure strain predictions would also improve. However, the results do indicate that the failure criteria are able to predict ply failure for a variety of fiber orientations and strain rates if the deformation response is predicted correctly. The results also indicate that even when some approximations and correlations are required in determining the ply failure strengths, reasonable results can still be obtained.

Table 1. Failure stress predictions for AS4/PEEK at a strain rate of 1×10^{-5}/s.

	Predicted Failure Stress (MPa)	Experimental Failure Stress (MPa)	Predicted Failure Strain	Experimental Failure Strain
[30°] laminate	130	140	0.017	0.014
[45°] laminate	98	104	0.011	0.014

Table 2. Failure stress predictions for AS4/PEEK at a strain rate of 0.1/s.

	Predicted Failure Stress (MPa)	Experimental Failure Stress (MPa)	Predicted Failure Strain	Experimental Failure Strain
[30°] laminate	165	170	0.017	0.014
[45°] laminate	114	112	0.012	0.011

CONCLUSIONS

In this study, strain rate dependent inelastic constitutive equations based on the Ramaswamy–Stouffer state variable equations have been formulated and implemented numerically to model the nonlinear deformation of ductile polymers. The constitutive equations have been implemented within a mechanics of materials based micromechanics method. The Hashin failure criteria have also been included within the micromechanics equations to allow for the prediction of ply ultimate strengths. Verification studies have been conducted using an AS4/PEEK composite system. In all cases, the predicted results compare well to experimentally obtained values.

Future efforts will include implementing laminate theory into the micromechanics equations to allow for the analysis of multilayered composites. High strain rate experiments will be conducted on a representative polymer matrix composite, and the deformation model will be characterized and validated for high strain rate conditions. Detailed penetration and failure models including property degradation will be developed. The resulting deformation and failure models will then be implemented into a transient dynamic finite element code, to allow for the simulation of ballistic impact tests. Furthermore, the deformation model will be extended into the large deformation regime, and the developed techniques will be extended to the analysis of woven composites.

NOMENCLATURE

D_0 = inelastic material constant representing maximum inelastic strain rate
f_1 = material constant in original Ramaswamy–Stouffer equations
f_2 = material constant in original Stouffer equations controlling stress rate effect
J_2 = second invariant of deviatoric stress tensor
n = inelastic material constant representing rate dependence of material
q = inelastic material constant representing hardening rate of material
s_{ij} = deviatoric stress components
S_{ij} = compliance matrix components
t = current time
Δt = time increment
v_f = fiber volume ratio of composite
X_S = ply in-plane shear strength
X_T = ply longitudinal tensile strength
X_C = ply longitudinal compressive strength
Y_T = ply transverse tensile strength
Y_C = ply transverse compressive strength
y_n = variable to be integrated in Runge-Kutta integration algorithm
Z_0 = material constant representing initial isotropic hardness of material
α = scaling factor for shear components of K_2 effective stress
β = material constant used in scaling shear components of K_2 effective stress
ε_{ij} = strain tensor components
ε_{ij}^I = inelastic strain components
ε_e^I = effective inelastic strain
$\dot{\varepsilon}_0$ = total applied strain rate in constant strain rate uniaxial tensile test
ε_S^I = inelastic strain at saturation in constant strain rate uniaxial tensile test

γ_{ij} = engineering shear strain components
Ω_{ij} = back stress component
Ω_m = inelastic material constant representing value of back stress at saturation
σ_{ij} = stress tensor components
σ_m = mean or hydrostatic stress
σ_s = saturation stress in constant strain rate uniaxial tensile test
$\dot{}$ = quantities with dots above them represent rates

Subscripts

A_f = bottom left subregion of composite unit cell (fiber material)
$M1$ = bottom right subregion of composite unit cell (matrix material)
$M2$ = top left subregion of composite unit cell (matrix material)
$M3$ = top right subregion of composite unit cell (matrix material)
$R1$ = region of composite unit cell consisting of subregions A_f and $A1$
$R2$ = region of composite unit cell consisting of subregions $M21$ and $M32$
$C1$ = region of composite unit cell consisting of subregions A_f and $M21$
$C2$ = region of composite unit cell consisting of subregions $M1$ and $M32$
f = fiber related material property
m = matrix related material property
12 = in-plane shear stress or strain components
11, 22, 33 = normal stress or strain components

REFERENCES

1. Harding, J. and Welsh, L.M. (1983). *J. Materials Science*, **18**: 1810–1826.
2. Daniel, I.M., Hsiao, H.M. and Cordes, R.D. (1995). Dynamic response of carbon/epoxy composites. In: *High Strain Rate Effects on Polymer, Metal and Ceramic Matrix Composites and Other Advanced Materials*. AD-Vol. 48. ASME.
3. Daniel, I.M., Hamilton, W.G. and LaBedz, R.H. (1982). Strain rate characterization of unidirectional graphite/epoxy composite. Composite Materials: Testing and Design (6th Conference). ASTM STP 787. American Society of Testing and Materials.
4. Weeks, C.A. and Sun, C.T. (1995). Nonlinear rate dependence of thick-section composite laminates. In: *High Strain Rate Effects on Polymer, Metal and Ceramic Matrix Composites and Other Advanced Materials*. AD-Vol. 48. ASME.
5. Thiruppukuzhi, S.V. and Sun, C.T. (1997). A viscoplasticity model for high strain rate characterization of polymeric composites. In: *Proceedings of the American Society of Composites Twelfth Technical Conference*. Lancaster, PA: Technomic Publishing Co., Inc.
6. Aidun, J.R. and Addessio, F.L. (1996). *J. Composite Materials*, **30**: 248–280.
7. Agarwal, B.D. and Broutman, L.J. (1990). *Analysis and Performance of Fiber Composites*. New York: John Wiley and Sons, Inc.
8. Daniel, I.M. and Ishai, O. (1994). *Engineering Mechanics of Composite Materials*. New York: Oxford University Press, Inc.
9. Stabb, G.H. (1999). *Laminar Composites*. Boston, MA: Butterworth-Heinemann.
10. Hashin, Z. (1980). *J. Applied Mechanics*, **47**: 329–334.
11. Chang, F.-K., Scott, R.A. and Springer, G.S. (1984). *J. Composite Materials*, **18**: 464–477.
12. Rotem, A. (1998). *Composites Science and Technology*, **58**: 1083–1094.
13. Yen, C.-F. (1998). Analysis of impact damage progression in composite structures. In: *Proceedings of the 5th International LS-DYNA Users Conference*. Southfield, MI.

14. Banerjee, R. (1992). Numerical simulation of impact damage in composite laminates. In: *Proceedings of the American Society for Composites Seventh Technical Conference*. Lancaster, PA: Technomic Publishing Co., Inc.
15. Langlie, S. and Cheng, W. (1989). Numerical simulation of high velocity impact on fiber-reinforced composites. In: *ASME Pressure Vessels and Piping Division (Publication) PVP*. Vol. 159. ASME.
16. Rosen, S.L. (1982). *Fundamental Principles of Polymer Materials*. New York: John Wiley & Sons.
17. Ward, I.M. (1983). *Mechanical Properties of Solid Polymers*. New York: John Wiley & Sons.
18. Stouffer, D.C. and Dame, L.T. (1996). *Inelastic Deformation of Metals. Models, Mechanical Properties and Metallurgy*. New York: John Wiley and Sons.
19. Valisetty, R.R. and Teply, J.L. (1992). *J. Composite Materials*, **26**: 1708–1724.
20. Zhang, C. and Moore, I.D. (1997). *Polymer Engineering and Science*, **37**: 414–420.
21. Bodner, S.R. (1987). Review of a unified elastic-viscoplastic theory. *Unified Constitutive Equations for Creep and Plasticity*. Barking, Essex, England: Elsevier.
22. Bordonaro, C.M. (1995). Rate dependent mechanical behavior of high strength plastics: experiment and modeling. PhD Dissertation, Rensselaer Polytechnic Institute, Troy, New York.
23. Goldberg, R.K. (1999). Strain rate dependent deformation and strength modeling of a polymer matrix composite utilizing a micromechanics approach. PhD Dissertation, University of Cincinnati, Cincinnati, Ohio.
24. Kreyszig, E. (1992). *Advanced Engineering Mathematics*. 7th edn. New York: John Wiley & Sons.
25. Sun, C.T. and Chen, J.-L. (1991). *Composites Science and Technology*, **40**: 115–129.
26. Robertson, D.D. and Mall, S. (1993). *Journal of Composites Technology and Research*, **15**: 181–192.
27. Pindera, M.-J. and Bednarcyk, B.A. (1999). *Composites: Part B*, **30**: 87–105.
28. Pecknold, D.A. and Rahman, S. (1994). *Computers & Structures*, **51**: 163–179.
29. Murthy, P.L.N. and Chamis, C.C. (1986). NASA TP-2515. National Aeronautics and Space Administration.
30. Coquill, S.L. and Adams, D.F. (1989). NASA CR-18105. National Aeronautics and Space Administration.

BIOGRAPHIES

Robert K. Goldberg

Robert K. Goldberg has been an aerospace engineer in the Structures and Acoustics Division of NASA Glenn for the past ten years. He received his PhD in Aerospace Engineering from the University of Cincinnati. He has over 20 technical publications. His areas of interest include the areas of constitutive modeling, composite mechanics and micromechanics, and high strain rate deformation and failure analysis.

Donald C. Stouffer

Donald C. Stouffer is Professor Emeritus of Aerospace Engineering and Engineering Mechanics at the University of Cincinnati, and has lectured on the Ohio Aerospace Institute television network, and at the University of Melbourne and Monash University in Australia. He has been active in constitutive modeling and life modeling of high-temperature super-alloys, metal–matrix composites, polymers, single crystal alloys, biological materials and tissues, and has published and lectured widely in the field. Professor Stouffer has worked for the US Air Force, General Electric Aircraft Engines, and the Aeronautical Research Laboratories in Australia.